Optically stimulated luminescence dating of Palaeolithic cave sites and their environmental context in the western Mediterranean

Dörschner, N.

Appendix A

Supplementary information of Doerschner et al. (2016), PLoS ONE

S1 File

MSA/MP nomenclature in the Maghreb.

The Maghreb (comprising Morocco, Algeria, Tunisia and western Libya) is geographically located in the transition zone between the Middle/Upper Paleolithic (MP/UP) industries of western Eurasia and the African MSA/LSA [1]. The geographical position and characteristics of stone tool morphologies of the Maghreb inevitably raise the question regarding nomenclature for the Palaeolithic technocomplexes in the region. Although recent papers invest much effort into resolving the ongoing scientific debate by providing critical reviews on the characteristics of these stone tool assemblages [2, 3], an overall accepted terminology for the Palaeolithic industries from the Maghreb has yet to be agreed upon. Dibble et al. [2] pointed out that the attribution of many assemblages from Morocco to the MP seem to have happened largely due to historical reasons, and that they moreover share closer affinity to other MSA industries from the African continent. For our paper, we decided to use the African terminology and consequently use the terms MSA and LSA for the respective Palaeolithic industries from the Maghreb.

References

1. Garcea EAA. The Spread of Aterian Peoples in North Africa. In: Garcea EAA, editor. South-Eastern Mediterranean Peoples Between 130,000 and 10,000 Years Ago. Oxford: Oxbow Books; 2010. p. 37-53.

2. Dibble HL, Aldeias V, Jacobs Z, Olszewski DI, Rezek Z, Lin SC, et al. On the industrial attributions of the Aterian and Mousterian of the Maghreb. Journal of Human Evolution. 2013;64(3):194-210. doi: http://dx.doi.org/10.1016/j.jhevol.2012.10.010.

3. Linstädter J, Eiwanger J, Mikdad A, Weniger G-C. Human occupation of Northwest Africa: A review of Middle Palaeolithic to Epipalaeolithic sites in Morocco. Quaternary International. 2012;274:158-74.

S2 File: Sediment and bedrock analyses

Grain size

Subsamples of 10 g (<2 mm diameter) were treated with hydrogen peroxide (50 ml, 35%) overnight and heated during the next day to remove any organic matter. Afterwards, the samples were dispersed using sodium pyrophosphate solution (10 ml, 0.4 N) and ultrasonic treatment for 45 minutes. Carbonates were not dissolved, in order to retain the original grain sizes of each sample. Particle-size analysis of the sand fraction was carried out by dry-sieving with screens of 63, 125, 200 and 630 µm. The subfractions of silt and clay were determined by X-ray granulometry using a SediGraph IIITM with MasterTech 052 AutosamplerTM (Micrometrics) [1].

XRF analysis

XRF analyses were applied to sediment samples and bedrock materials to obtain their elemental compositions. Concentrations of specific elements and their ratios can serve as indicators for sediment provenience and weathering processes.

Bedrock materials were put in a steel cylinder, closed with a steel pin and crushed manually by hammering on the steel pin. The crushed bedrock samples and subsamples of the air-dried sediments (8 g, <2 mm diameter) were homogenised and milled to fine powder (<30 µm) using a vibration mill MM 200 (Retsch) for 10 min at 30 Hz). 4 g of the milled powder was mixed and homogenised with a binder (1 g Cereox Licowax). Subsequently, the mixture was filled into a die and pressed to pellets by a Vaneox press (20 t for 2 min). Analyses were carried out with a Spectro Xepos X-ray fluorescence analyser under a He gas atmosphere. Contents of the elements from sodium (11) to uranium (92) were simultaneously determined.

Thin sections

For the preparation of thin sections, samples were first impregnated with araldite glue and then placed in a vacuum (-20 in Hg) overnight. After being oven dried, both the samples and the glass slides were ground down to create flat surfaces using a Metaserv 2000 grinder. The samples were mounted onto the slides before being cut and then ground down using the diamond wheel on a PetroThin machine until a uniform thickness of 30 µm was achieved. Visual examinations were performed under a Nikon polarizing microscope using both plane-polarized and cross-polarized light (see the sections on micromorphological characteristics in Nash and McLaren [2] and the references therein).

Stable isotopes

For stable isotope analysis hand specimens were ground in a mortar using a pestle and then powdered in a ball mixer mill. About 1.5 mg per sample were flushed with He to remove air and then acidified with ~0.2 ml phosphoric acid (100%). CO_2 gas from the acidified samples was obtained using a Gilson autosampler system. Measurements were conducted using a SERCON Hydra 20-20 continuous flow isotope ratio mass spectrometer, calibrated via IAEA calcite standard CO8. The precision of carbonate analysis based on replicate investigation of the laboratory standard is better than 0.2‰ for both $\delta^{18}O$ and $\delta^{13}C$. Isotope values are reported per mil (‰) vs V-PDB.

References

1. Zielhofer C, Clare L, Rollefson G, Wächter S, Hoffmeister D, Bareth G, et al. The decline of the early Neolithic population center of 'Ain Ghazal and corresponding earth-surface processes, Jordan Rift Valley. Quaternary Research. 2012;78(3):427-41. doi: http://dx.doi.org/10.1016/j.yqres.2012.08.006.

2. Nash DJ, McLaren SJ, editors. Geochemical Sediments and Landscapes. Oxford: Blackwell; 2007.

Supplementary Tables

S1 Table
Measured moisture contents, beta dose rates and chosen preheat/cutheat temperatures.

Sample	Unit	Depth	Moisture content (%)		Attenuated beta dose rate (Gy/ka)		Preheat/Cutheat
		(cm)	Full saturation	Present day	Beta counter	HRGS[b]	
Cave mouth section							
L-EVA-1210	1	40	19.8	5.5[a]	0.90±0.02	0.70±0.02	260/220
L-EVA-1139	3a	55	22.9	0.9	0.73±0.01	0.74±0.01	260/220
L-EVA-1140	3b	70	22.4	1.1	0.69±0.03	0.40±0.02	260/220
L-EVA-1141	4c	110	19.2	2.2	0.68±0.01	0.56±0.01	240/200
Lower cave section							
L-EVA-1142	6d	185	24.3	1.9	1.49±0.02	2.55±0.05	260/220
L-EVA-1143	16	210	24.3	5.5	1.74±0.05	1.71±0.03	260/220
L-EVA-1083	30	260	26.8	9.3	2.32±0.05	1.99±0.04	260/220
L-EVA-1084	39	300	25.2	9.5	1.87±0.03	1.71±0.04	260/220
L-EVA-1085	55	375	26.7	5.2	1.81±0.03	1.50±0.03	260/220
L-EVA-1144	55	375	26.7	5.5	1.72±0.04	1.58±0.03	260/220
Terrace section							
L-EVA-1145	S2	45	25.0	12.1[a]	0.76±0.02	0.89±0.02	260/220
L-EVA-1146	S3	70	24.5	4.1[a]	0.79±0.01	0.73±0.02	260/220
L-EVA-1212	S5	100	19.4	4.1[a]	0.62±0.01	0.49±0.01	260/220
L-EVA-1213	S6	115	17.0	3.6[a]	0.93±0.02	0.51±0.02	260/220
L-EVA-1148	S7	150	23.8	8.1[a]	0.81±0.02	0.84±0.02	260/220

[a]Samples were collected after a rain event.
[b]High resolution gamma spectrometry.

S2 Table

Summary of faunal remains.

Linnaean Names	Vernacular Names	MIS 1	MIS 2		MIS 3		MIS 5			MIS 6			Wengler's
		1[a]	S2[a]	S3[a]-S4[b]	S5[a]	3a[a]	S6[a]	3b[a]	S7[a]	4ab[b]	4c[a]	5[b]	Unit III[b]
Hystrix cristata	crested porcupine	2											
Lepus sp.	hare	1		1									
Felis cf. *caracal*	cf. caracal	1											
Canis sp.	dog or jackal	1											1
Equus sp.	indet. equid	13	35	5	1	1		2	10	2	3	4	24
Rhinocerotidae gen. et sp. indet.	rhinoceros	1						1			1		2
Suidae gen. et sp. indet.	pig(s)	3											
Sus sp.	pig	3											
Phacochoerus africanus	warthog						1						
Gazella sp.	gazelle	5	6	1							1		1
Caprini	sheep/goat	6											
Ammotragus lervia	Barbary sheep/aoudad		1										
Alcelaphini gen. et sp. indet.	hartebeest/wildebeest	19	21										14
Bovini gen. et sp. indet.	bovine	1	4						1				1
	Small bovid(s)	35	23		2	2							4
	Small-medium bovid(s)	92	55	2	1		1		1		1	1	10
	Large-medium bovid(s)	38	66	4		2					2	3	38
	Large bovid(s)	9	11				1	2			2		16
NISP		230	222	13	4	5	3	5	12	2	10	8	115
	Coprolite											2	4
Aves	Bird												1
Struthio camelus	Ostrich eggshell	18	6							1			3
	Terrestrial tortoise	18	4		1		1						1
	Terrestrial mollusk	122	8	2	4				2				

[a]Layer dated in this study.

[b]Chronological position is undetermined.

S3 Table

Single grain characteristics.

Sample	n[a]	No signal[b]	T_N signal <3x BG	No L_N/T_N intersection	Dim grains[c]	Recuperation >5%	Poor recycling ratio (>20%)	Depletion by IR	D_e error >30%	Grubbs test[d]	accepted grains	
	(100%)	(%)	(%)	(%)	(%)	(%)	(%)	(%)	(%)	(%)	total	(%)
Cave mouth section												
L-EVA-1210	4100	76.2	0.2	3.2	12.1	0.1	3.1	3.4	0.2	0.1	54	1.3
L-EVA-1139	1000	47.9	0	7.1	14.6	0.4	9.0	11.7	2.4	0.2	67	6.7
L-EVA-1140	900	54.0	0	5.8	14.4	0.2	7.3	9.4	1.7	0.2	62	6.9
L-EVA-1141	1000	52.5	0.2	17.9	4.3	2.2	5.7	10.1	0.5	0	66	6.6
Terrace section												
L-EVA-1145	1200	57.9	0.2	1.3	16.9	0.4	8.5	9.8	0.1	0.1	58	4.8
L-EVA-1146	1300	69.1	0.2	1.9	11.5	0.6	4.9	6.5	0.2	0	68	5.2
L-EVA-1212	1400	66.3	0	2.4	9.9	0.2	6.1	9.6	0.8	0	64	4.6
L-EVA-1213	1500	67.3	0.3	7.9	7.3	0.4	4.5	7.2	1.1	0	59	3.9
L-EVA-1148	800	33.9	0.1	19.3	13.0	1.9	7.8	13.5	2.8	0	63	7.9

[a]Total number of grains measured per sample.

[b]Percentage of grains not emitting any detectable luminescence signal.

[c]Percentage of grains rejected due to insufficient test-dose signal.

[d]Percentage of grains identified as statistical outliers [1].

1. Grubbs FE. Sample Criteria for Testing Outlying Observations. 1950:27-58. doi: 10.1214/aoms/1177729885.

S4 Table
Single grain dose recovery properties.

Sample	Unit	accepted/measured grains	given dose (Gy)	measured D_e [a] (Gy)	Overdispersion (%)	recovery ratio
Cave mouth section						
L-EVA-1210	1	51/1600	11.2	10.9	2±4	0.97±0.04
L-EVA-1139	3a	86/1000	78.5	72.2	7±1	0.92±0.05
L-EVA-1140	3b	58/900	98.5	90.6	14±2	0.92±0.06
L-EVA-1141	4c	97/800	105.0	100.8	5±1	0.96±0.05
Terrace section						
L-EVA-1145	S2	88/1200	21.5	20.9	7±1	0.97±0.05
L-EVA-1146	S3	86/1400	23.9	22.9	7±1	0.96±0.05
L-EVA-1212	S5	61/900	67.2	63.8	6±1	0.95±0.05
L-EVA-1213	S6	63/900	118.3	111.2	14±2	0.94±0.07
L-EVA-1148	S7	89/800	135.2	124.4	9±1	0.92±0.05

[a]Determined using the Central Age Model (Galbraith et al., 1999).

S5 Table

Grain size results.

Sample	Layer	Grain size fractions (%)												
		fT	mT	gT	fU	mU	gU	fS	mS	gS	Total clay (T)	Total silt (U)	Total sand(S)	classified as [1, 2]
Cave mouth section														
L-EVA-1210	1	8.4	3.7	8.0	6.9	9.4	8.4	20.8	18.3	16.0	20.1	24.7	55.2	muddy Sand
L-EVA-1139	3a	4.3	1.1	2.9	2.9	3	2.9	8.0	12.9	62.0	8.3	8.8	82.9	muddy Sand
L-EVA-1140	3b	-[a]	-[a]	-[a]	-[a]	-[a]	-[a]	-[a]	-[a]	-[a]	-[a]	-[a]	-[a]	-[a]
L-EVA-1141	4c	6.8	2.4	7.1	6.7	4.4	4.5	13.7	15.8	38.6	16.3	15.6	68.1	muddy Sand
Lower cave section														
L-EVA-1142	6d	9.7	4.4	6.3	8.9	6.1	5.3	13.2	14.5	31.6	20.4	20.3	59.3	muddy Sand
L-EVA-1143	16	13.9	6.6	8.3	11.3	8.4	10.0	19.4	8.8	13.3	28.8	29.7	41.5	sandy Mud
L-EVA-1083	30	7.9	3.3	22.1	15.1	9.6	9.6	16.2	7.1	9.1	33.3	34.3	32.4	sandy Mud
L-EVA-1084	39	12.9	10.2	7.3	9.5	7.6	11.7	22.4	11.2	7.2	30.4	28.8	40.8	sandy Mud
L-EVA-1085	55	15.8	6.3	6.6	6.4	5.8	10.1	25.9	14.7	8.4	28.7	22.3	49.0	sandy Mud
L-EVA-1144	55	14.6	7.0	6.6	5.7	5.1	9.3	25.5	14.7	11.6	28.2	20.1	51.7	muddy Sand
Terrace section														
L-EVA-1145	S2	6.2	4.8	8.0	7.0	5.0	7.3	26.2	23.9	11.6	19.0	19.3	61.7	muddy Sand
L-EVA-1146	S3	10.1	7.6	9.4	7.0	5.1	6.9	21.8	17.3	14.9	27.1	19.0	53.9	muddy Sand
L-EVA-1212	S5	9.3	6.2	9.3	6.4	4.5	4.0	15.9	22.5	22.0	24.8	14.9	60.3	muddy Sand
L-EVA-1213	S6	11.7	5.2	7.0	6.2	4.5	4.4	16.3	20.7	24.0	23.9	15.1	61.0	muddy Sand
L-EVA-1148	S7	9.6	6.2	9.0	7.5	4.9	5.5	20.5	22.7	14.1	24.8	17.9	57.3	muddy Sand

[a]Not enough sample material for grain size determination available.

1. Folk RL. The distinction between grain size and mineral composition in sedimentary rocks. Journal of Geology. 1954;62:344-59.
2. Folk RL. Petrology of Sedimentary Rocks. Austin, TX: Hemphill Publishing; 1980. 184 p.

S6 Table

XRF results and $CaCO_3$ content.

Sample	S	Cl	Mg	Ca	Al	Fe	Na/Cl 10^0	Pb/Al 10^{-3}	Rb/K 10^{-3}	Ni/Al 10^{-3}	Ti/Th 10^3	K/Al 10^0	$CaCO_3$
	(g/kg)						mol ratio						(%)
Cave mouth section													
L-EVA-1210	0.56	0.20	32.0	207	20.3	15.0	52.4	3.36	3.15	0.97	0.27	0.42	56
L-EVA-1139	0.65	0.16	20.5	273	14.8	9.8	67.0	2.48	3.91	3.12	0.21	0.39	78
L-EVA-1140	0.55	0.23	20.2	261	14.9	9.9	41.4	2.88	3.86	2.71	0.22	0.39	89
L-EVA-1141	0.52	0.20	19.7	254	18.7	11.7	46.7	1.57	3.81	1.37	0.23	0.35	62
Lower cave section													
L-EVA-1142	2.18	4.59	27.7	197	23.5	14.9	3.3	0.96	1.54	0.93	0.30	0.93	61
L-EVA-1143	2.92	0.96	25.6	130	44.5	23.9	10.5	0.77	2.82	0.63	0.41	0.42	33
L-EVA-1083	3.21	11.3	42.3	92	40.2	23.9	1.7	1.17	2.13	0.70	0.38	0.61	26
L-EVA-1084	2.62	4.09	29.6	88	47.7	25.0	5.0	1.09	2.54	0.66	0.39	0.45	19
L-EVA-1085	0.44	1.86	25.5	61	53.9	26.9	5.8	0.82	2.43	0.55	0.44	0.41	34
L-EVA-1144	0.88	1.02	26.3	85	49.9	26.1	12.9	0.87	2.50	0.57	0.46	0.40	21
Terrace section													
L-EVA-1145	0.64	0.19	29.0	168	31.3	17.3	69.4	12.18	3.37	0.67	0.32	0.30	35
L-EVA-1146	0.34	0.11	20.9	207	28.0	16.4	61.0	2.50	4.00	0.80	0.30	0.29	45
L-EVA-1212	0.30	0.11	20.9	240	18.3	10.7	77.1	1.93	3.85	0.89	0.25	0.29	79
L-EVA-1213	0.30	0.10	19.9	186	33.2	19.0	90.3	1.14	3.73	0.89	0.34	0.27	66
L-EVA-1148	0.21	0.12	20.4	191	33.7	17.9	79.5	0.93	3.62	0.81	0.36	0.27	34

S7 Table
Summary of istope data.

Sample	$\delta^{13}C$ (‰)	$\delta^{18}O$ (‰)
Calcrete		
2iii	-7.65	-5.03
3i	-6.67	-6.61
3iii	-6.79	-6.33
4ii	-6.56	-6.23
5i	-4.31	-6.84
5ii	-4.87	-7.31
mean	**-6.14**	**-6.39**
standard deviation	**1.16**	**0.70**
Organic layer		
3iii	-2.85	-8.16
4i	-1.21	-9.48
mean	***-2.03***	***-8.82***
standard deviation	***1.64***	***0.66***
Laminar crust		
5iii	-9.12	-5.33

S8 Table

FMM details.For L-EVA-1139 and L-EVA-1140 BIC and llik continuously increase and decrease, respectively, when Overdispersion values further increase. The chosen combination of Overdispersion and number of components used for age determination of each sample are shaded in grey.

Sample	k	σ_{OD}[1]	K1		K2		K3		BIC	llik
			D_e±error	Proportion	D_e±error	Proportion	D_e±error	Proportion		
L-EVA-1210	2	15	3.2±0.1	7.1%	10.9±0.3	92.9%			62.1	-25.09
	2	20	3.0±0.1	6.3%	10.8±0.4	93.7%			54.2	-21.13
	2	25	2.7±0.1	4.8%	10.7±0.5	95.2%			52.7	-20.36
	2	30	1.8±0.5	2.4%	10.4±1.0	97.6%			53.6	-20.81
	3	15	1.6±0.1	1.9%	5.9±0.6	14.8%	11.4±0.6	83.3%	53.0	-16.47
	3	20	1.6±0.3	1.9%	5.5±0.7	10.7%	11.2±0.4	87.4%	53.6	-16.84
	3	25	1.6±0.3	1.9%	5.0±0.8	6.9%	10.9±0.4	91.2%	56.6	-18.35
	3	30	1.6±0.4	2.0%	4.8±1.1	3.6%	10.7±0.5	94.4%	60.7	-20.39
L-EVA-1139	2	15	71.3±14.1	42.2%	99.4±19.7	57.6%			23.0	-5.20
	2	20	72.3±30.0	28.3%	92.4±23.7	71.7%			24.5	-5.93
	3	15	51.3±24.3	3.5%	77.3±8.9	54.3%	103.7±9.2	42.2%	30.3	-4.64
	3	20	69.7±20.7	20.4%	89.5±NaN	45.5%	92.87±57.1	37.2%	30.9	-4.93
L-EVA-1140	2	15	57.2±3.4	25.9%	105.8±7.5	74.1%			55.9	-21.76
	2	20	56.7±4.6	23.1%	104.2±8.5	76.9%			51.4	-19.51
	2	25	57.1±13.5	19.9%	101.6±9.3	80.1%			53.0	-20.29
	3	15	53.4±7.7	19.3%	91.3±10.5	48.8%	122.9±12.5	31.9%	59.1	-19.23
	3	20	56.0±10.7	21.9%	97.0±12.2	38.1%	110.0±5.0	40.1%	59.6	-19.48
L-EVA-1141	2	15	59.1±2.4	21.6%	137.7±3.2	78.4%			133.0	-60.20
	2	20	56.7±3.0	18.6%	135.7±4.0	81.4%			106.2	-46.80
	2	25	55.2±3.4	16.4%	134.0±8.3	83.6%			96.1	-41.77
	2	30	53.6±7.3	13.7%	131.4±9.4	86.3%			99.3	-45.37
	3	15	50.8±7.5	14.3%	114.9±4.5	60.8%	191.6±7.9	24.9%	109.0	-44.03
	3	20	51.7±10.1	14.3%	118.2±6.0	65.4%	195.3±13.0	20.3%	103.0	-41.04
	3	25	51.9±13.9	13.5%	120.8±9.3	69.4%	188.1±23.1	17.1%	101.9	-40.46
	3	30	51.8±22.8	12.1%	115.6±NaN	35.1%	140.4±NaN	52.8%	101.6	-40.34

[1]Overdispersion used running the FMM.

Supplementary Figures

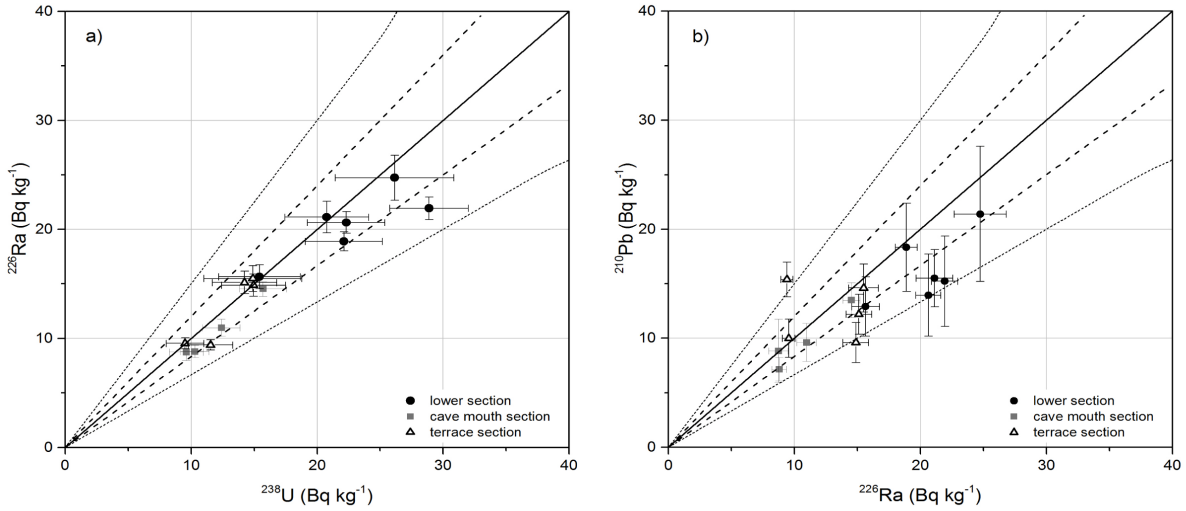

S1 Fig. Parent-daughter equilibrium plots for Rhafas. (a) 238U/226Ra (b) 226Ra/210Pb. In each figure the solid line represents secular equilibrium. Samples from the lower section, the cave mouth section and the slope section are shown as black dots, grey squares and open triangles respectively. Dashed lines represent 20% and dotted lines 50% of equilibrium.

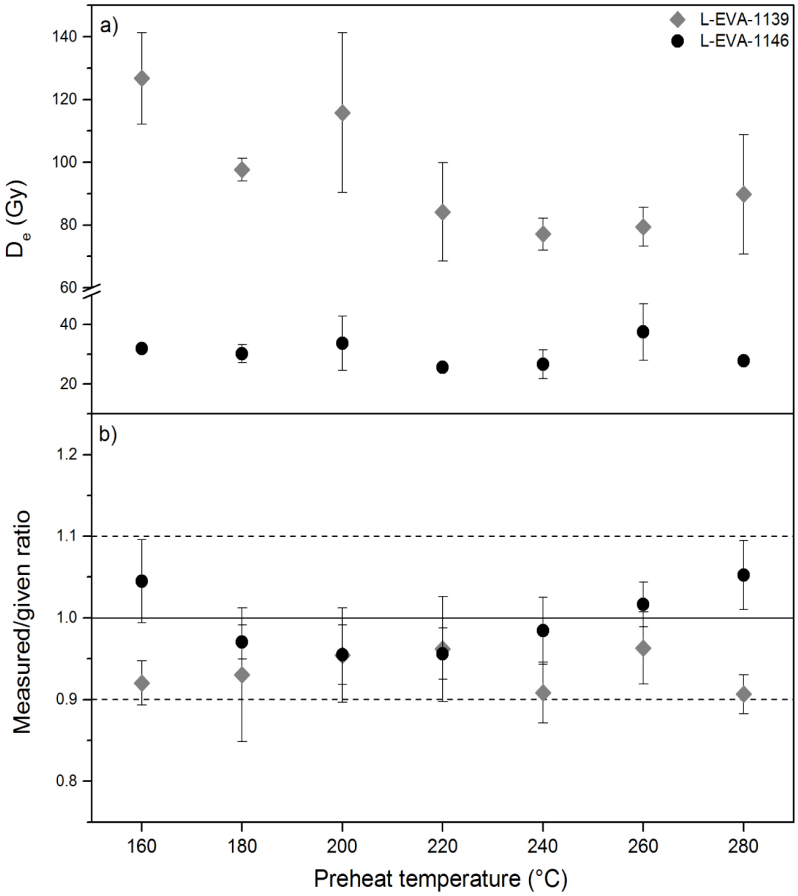

S2 Fig. Results of OSL standard performance tests. (a) Preheat plateau test (b) Dose-recovery preheat plateau test for samples L-EVA-1139 (grey diamonds) and L-EVA-1146 (black circles). The solid line indicates the target value; dashed lines represent 10% deviation from unity.

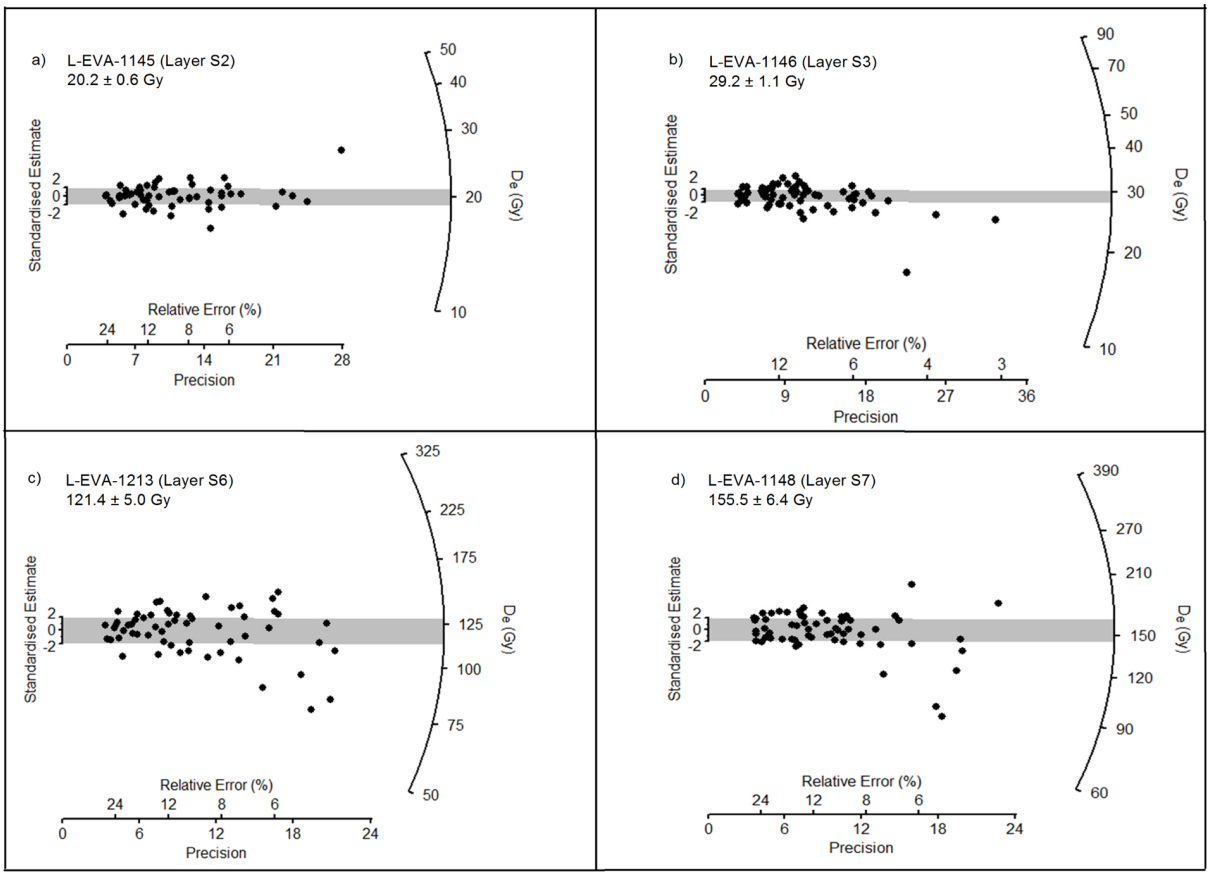

S3 Fig. Radial plots showing the dose distributions of single grain values of samples from the terrace section. (a) L-EVA-1145, (b) L-EVA-1146, (c) L-EVA-1213 and (d) L-EVA-1148. The shaded bands in the radial plots correspond to the standard error deviation from the calculated De.

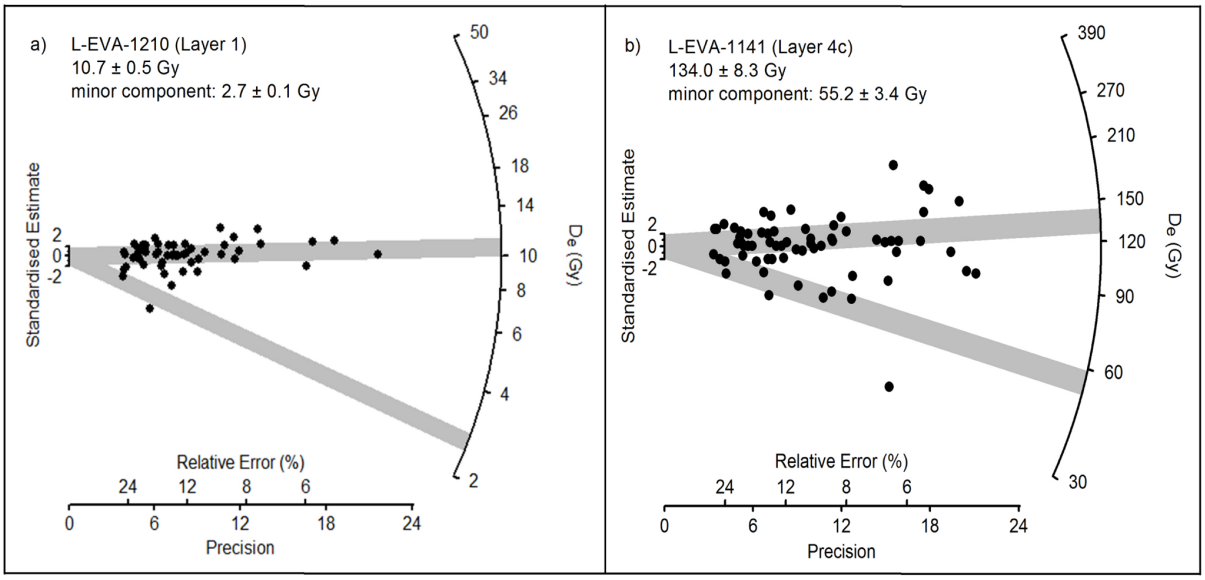

S4 Fig. Radial plots showing the dose distributions of single grain values of samples from the cave mouth section. (a) L-EVA-1210 and (b) L-EVA-1141. The shaded bands in the radial plots correspond to the standard error deviation from the calculated De for each identified component.

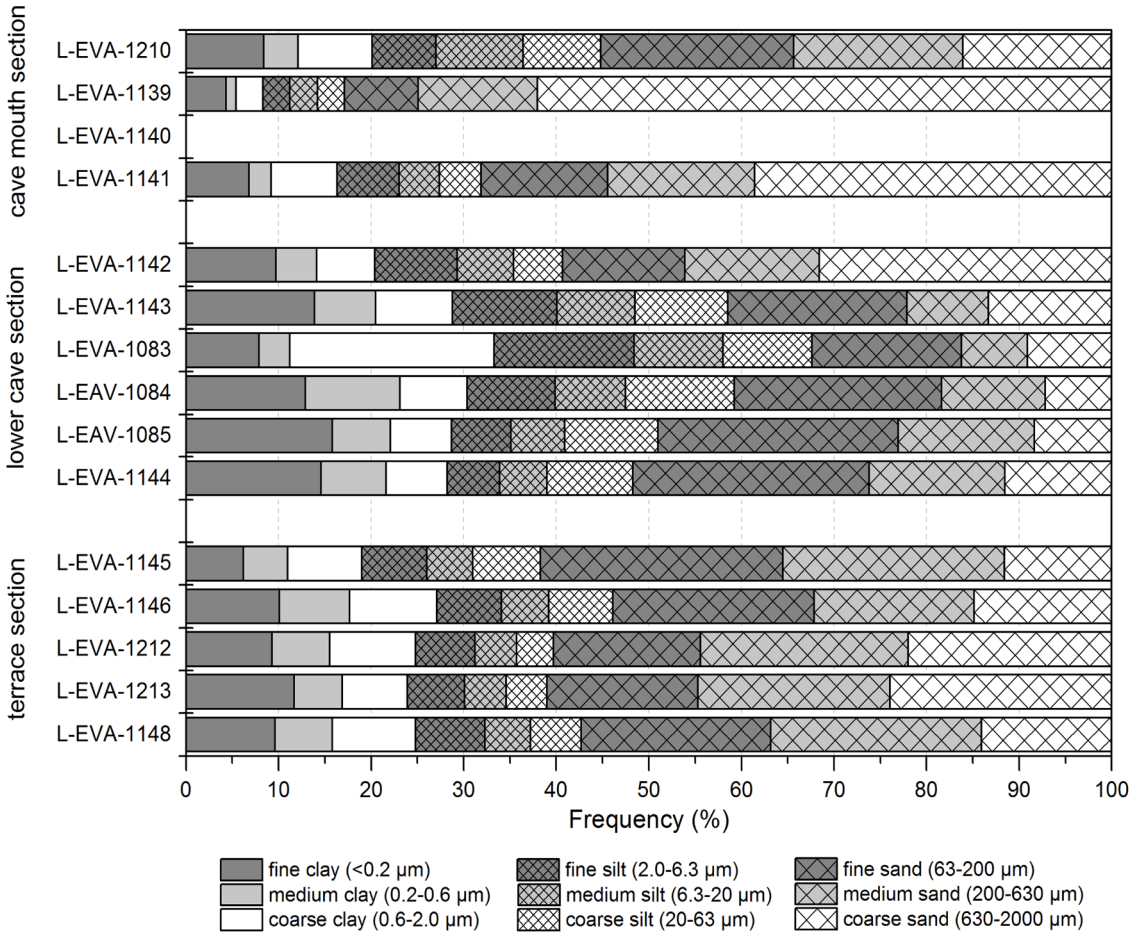

S5 Fig. Grain-size distributions of the OSL samples per section. Each stacked bar shows the percentage distribution of the grain-size classes for one sample (in total 100%).

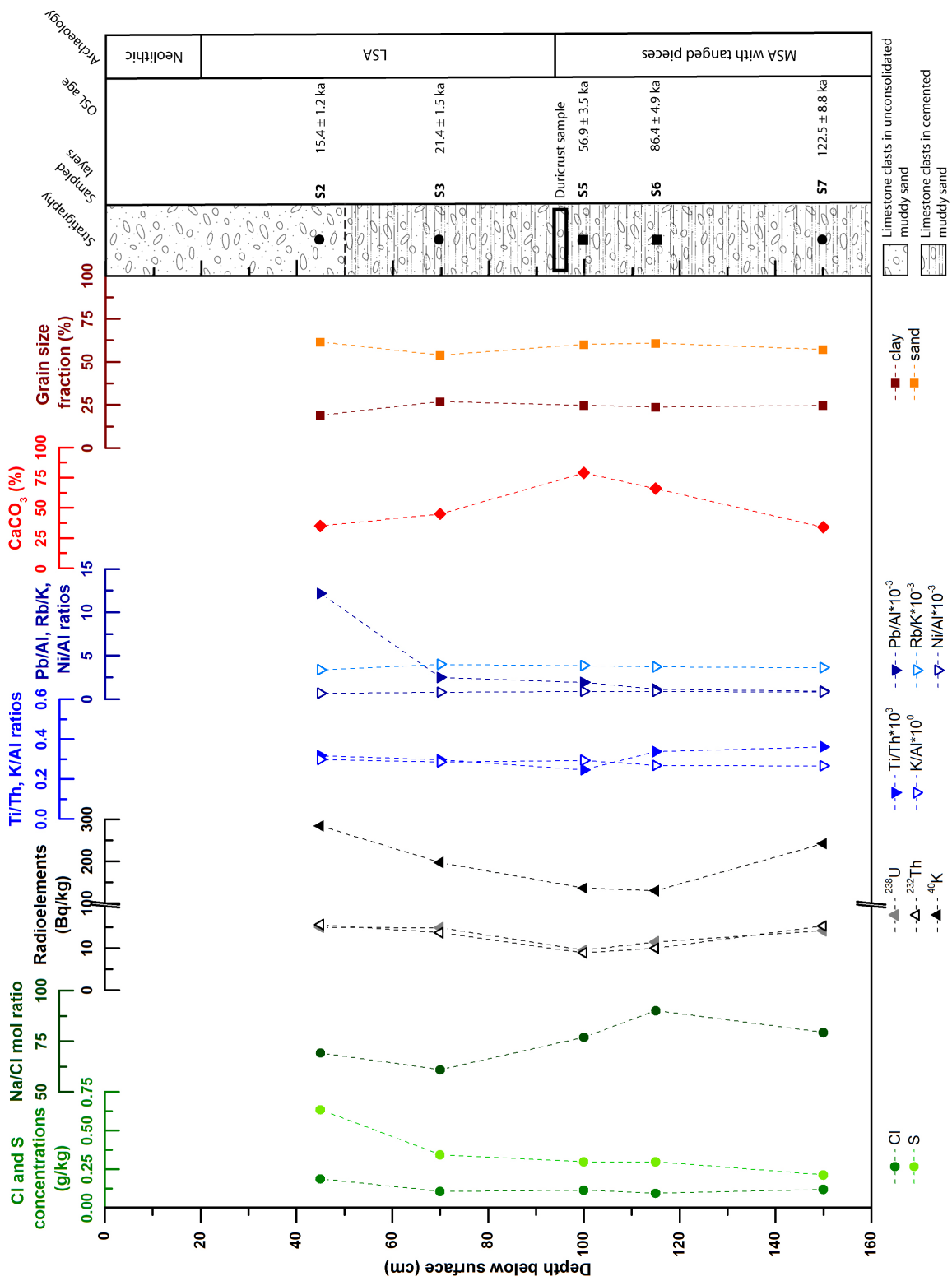

S6 Fig. Sedimentological characteristics of the terrace section.

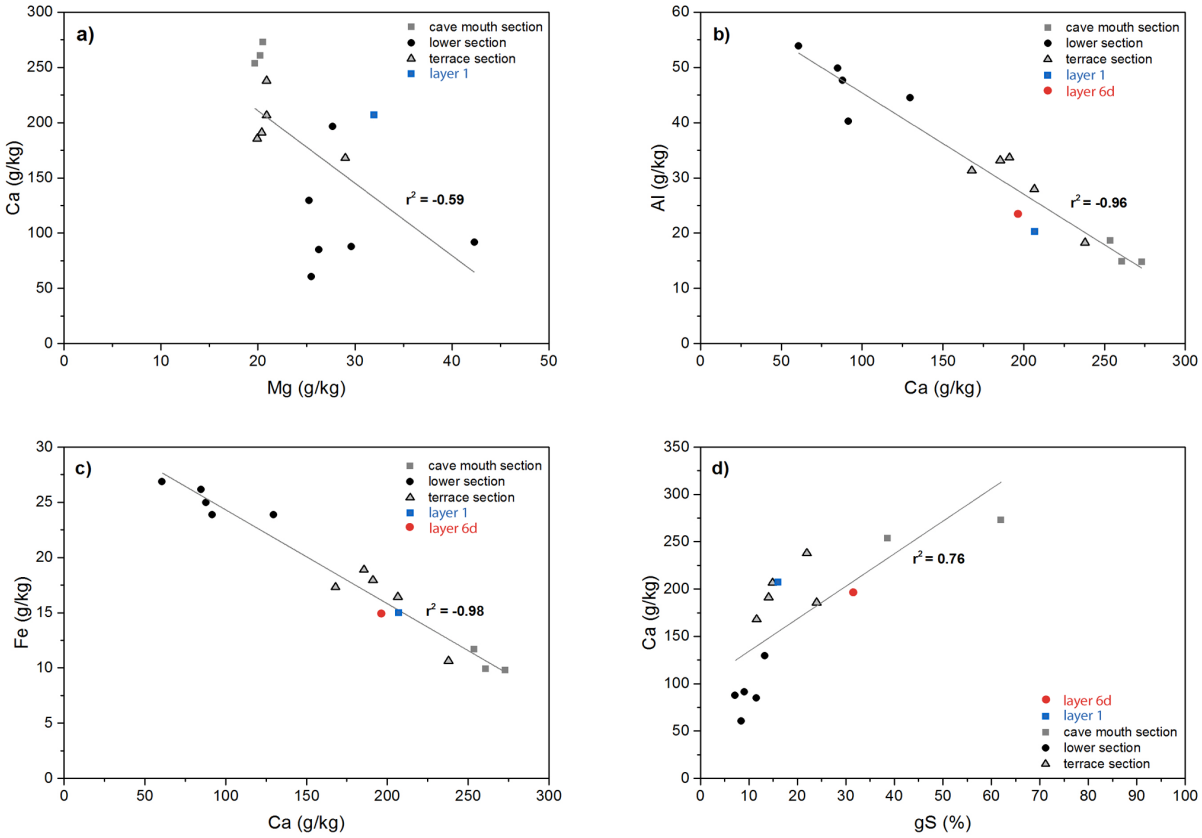

S7 Fig. XRF results showing correlations between Ca and Mg, Al and Ca, Fe and Ca, and Ca and gS. Layer 1 (blue square) and 6d (red dot) plot relatively far away from their groups, which indicates that they do not share the same sedimentological characteristics with the other layers of the cave mouth and the lower cave section, respectively.

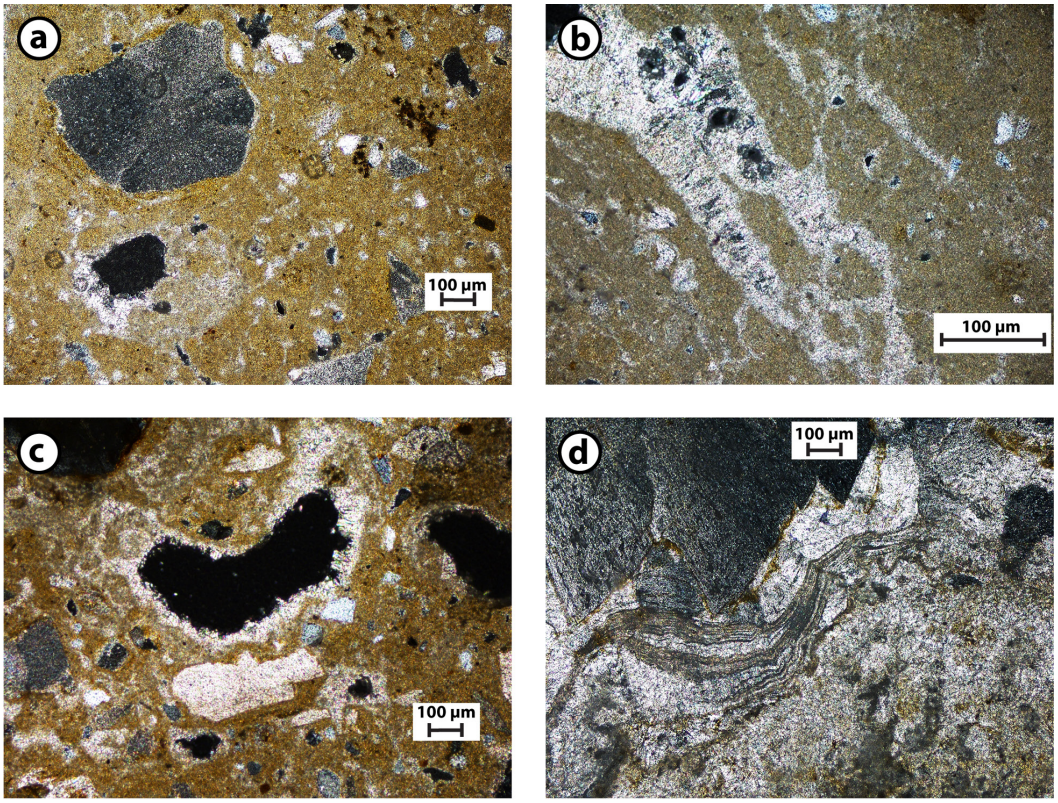

S8 Fig. Thin section photographs. (a) micritic cement with corroded lithoclasts: around one of the clasts there is evidence of the dissolution of some of the calcite cement and replacement by silica cement (arrow); (b) stringer within the silcrete-calcretes showing the chalcedony crystals in greater detail; (c) preservation of the form of a replaced calcite shell by silicification; (d) mammillary structured quartz crystals showing micro-laminated opal as well as fibrous lussatite and chalcedony. Photographs were taken under cross-polarised light.

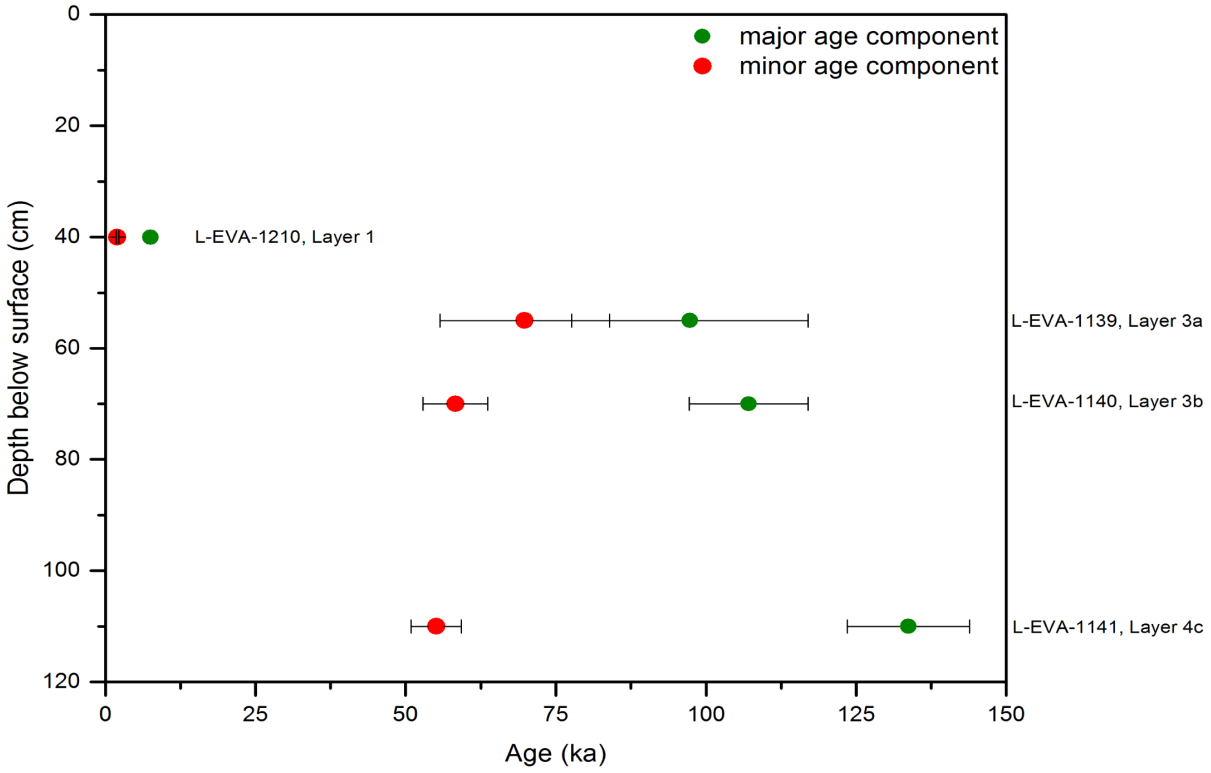

S9 Fig. Single grain OSL ages for the cave mouth section at Rhafas determined by applying the FMM. Major and minor age components are shown in green and red, respectively

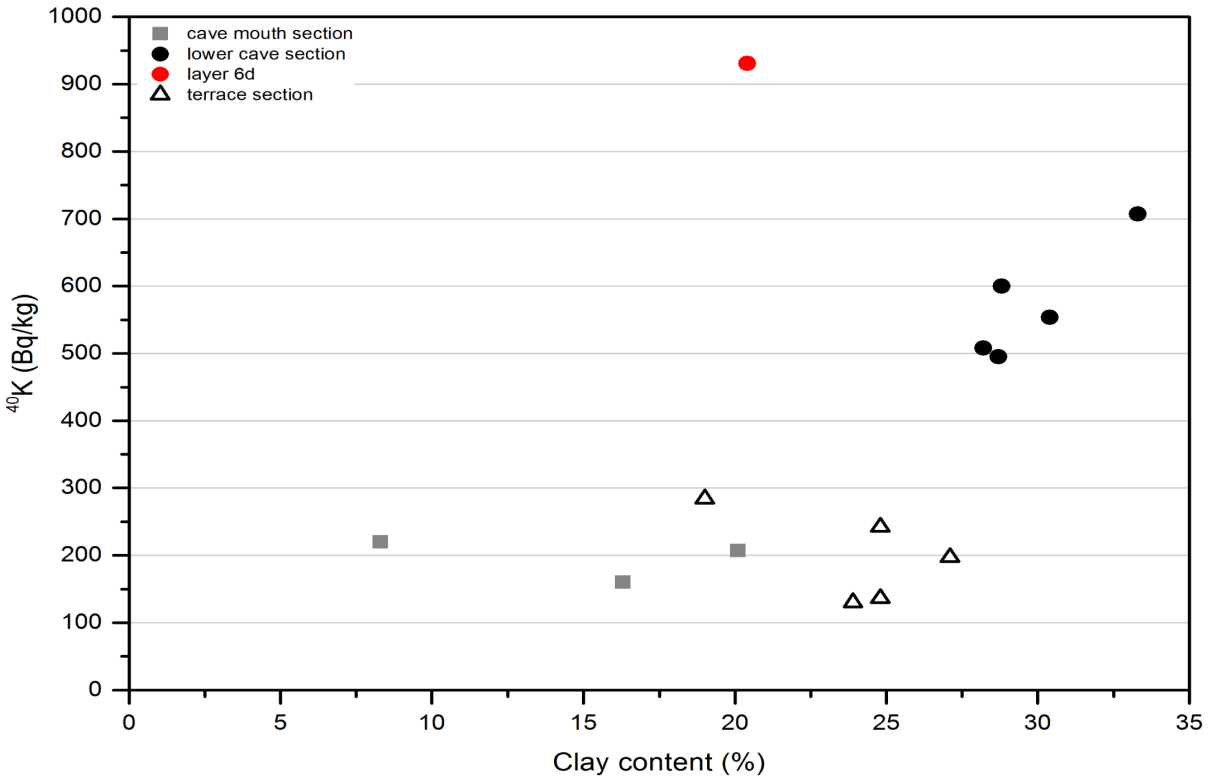

S10 Fig. Correlation between 40K and clay content at Rhafas.

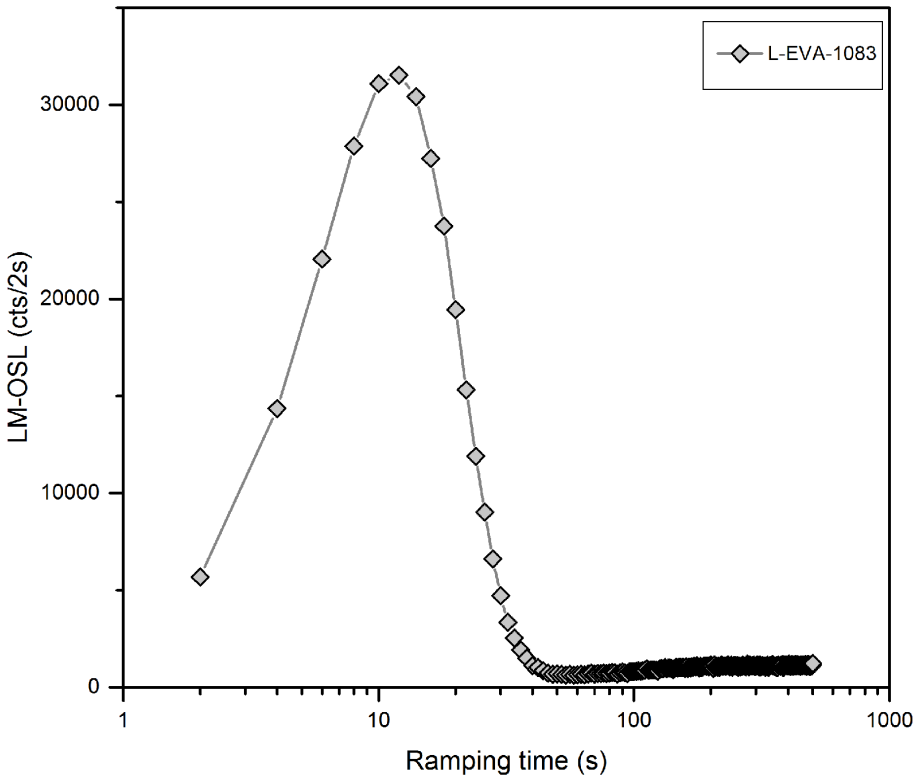

S11 Fig. LM-OSL curve for L-EVA-1083, showing dominant OSL fast component.